



## ORIGINAL ARTICLE

# Comprehensive characterization of narirutin metabolites *in vitro* and *in vivo* based on Analogous-Core recursion analysis strategy using UHPLC-Q-Exactive Orbitrap MS/MS



Shuyi Song<sup>a,1</sup>, Hongyan Zhou<sup>b,1</sup>, Xianming Lan<sup>a</sup>, Xiaoqing Yuan<sup>a</sup>, Yanan Li<sup>b</sup>, Shuteng Huang<sup>a</sup>, Zhibin Wang<sup>c,\*</sup>, Jiayu Zhang<sup>a,\*</sup>

<sup>a</sup> School of Pharmacy, Binzhou Medical University, 264003 Yantai, Shandong, China

<sup>b</sup> School of Pharmacy, Shandong University of Traditional Chinese Medicine, 250300 Jinan, Shandong, China

<sup>c</sup> Tongrentang Research Institute, Beijing 100079, China

Received 15 December 2022; accepted 24 April 2023

Available online 28 April 2023

## KEYWORDS

Narirutin;  
UHPLC-Q-Exactive Orbitrap MS/MS;  
Metabolites;  
Analogous-Core Recursion analysis strategy;  
*In vitro* and *in vivo*

**Abstract** Narirutin, extracted from the dried ripe pericarp of Rutaceae orange and its cultivated varieties, is a dihydroflavone compound with various biological activities and pharmacological effects. So far as we know, the metabolism profiling of narirutin has been insufficient until now. In the present study, an efficient method was employed to perform rapid analysis and identification of narirutin metabolites by using ultra-high performance liquid chromatography quadrupole exactive orbitrap MS/MS (UHPLC-Q-Exactive Orbitrap MS/MS) combined with an analogous core recursion (ACR) analysis strategy. Firstly, according to the basic core structure of the dihydroflavonoid, the cleavage mode and fragmentation ions of narirutin were summarized. Secondly, based on the difference of the substituent groups, the fragment ions of narirutin were preliminarily inferred and verified by the secondary mass spectra of its standard compound. Thirdly, the fragment ions of narirutin in positive and negative ion modes were summarized to provide a basis for the identification of metabolites. Fourthly, candidate metabolites were accurately and tentatively identified according to the cleavage law of mass spectrometry, literature reports, comparison of reference substances, and especially the diagnostic fragment ion clusters (DFICs) and characteristic suggestive ions (CSIs) deduced preliminarily. Finally, a total of 46 metabolites (30 *in vivo* and 19 *in vitro*), including prototype drugs were identified based on the ACR analysis strategy, chromatographic retention behavior of metabolites, corresponding ClogP value and accurate molecular weight. Among them, 22 metabolites were discovered in rats plasma, 12 in urine, 4 in liver tissue, 19 in liver microsomes, respectively. Additionally, metabolites relative contents were also studied by extracted ion chromatography (EIC) method. Our result also illustrated that narirutin primarily

\* Corresponding authors.

E-mail addresses: wangzhibin@tongrentang.com (Z. Wang), zhangjiayu0615@163.com (J. Zhang).

<sup>1</sup> The work has been contributed by these authors equally.

underwent glucuronidation, sulfation, glutathione binding, deglycosylation, oxidation, reduction, methylation, hydroxylation, ring-opening and their composite reactions. A novel strategy was constructed to comprehensively elucidate the biotransformation pathways of narirutin *in vitro* and *in vivo*, and a systematic metabolic profile of narirutin was generated. This study provided a great reference for further understanding of the biotransformation pathways and guiding for clinical application of narirutin.

© 2023 The Authors. Published by Elsevier B.V. on behalf of King Saud University. This is an open access article under the CC BY-NC-ND license (<http://creativecommons.org/licenses/by-nc-nd/4.0/>).

## 1. Introduction

Narirutin (Naringenin 7-O-rutinoside) attributed to dihydroflavone compounds (Duan et al., 2016) has been isolated from the dry and mature peel extract of orange (*Citrus reticulata* Blanco) as well as its cultivated varieties in Rutaceae. Plenty of studies have shown that Narirutin owns a great many of pharmacological activities, including blood pressure reduction (Fraga et al., 2021), glucose and lipid downregulation (Chiechio et al., 2021), antimicrobial (Shehata et al., 2021), anti-inflammatory (Ha et al., 2012), anti-virus (Yang et al., 2020), anti-tuberculosis (Sahu et al., 2020), anti-cancer (Lim et al., 2015) and anti-allergic (Niu et al., 2021) properties. At the same time, narirutin can improve the level of intracellular cAMP, stimulate endothelial nitric oxide synthase and activate voltage-gated potassium channels in vascular smooth muscle cells, thus playing a role in vascular relaxation (Wong et al., 2021). It also showed protective effects on the immune system and inflammation (Miles and Calder 2021), alcohol-induced liver damage (Park et al., 2013) and gastric Injury (Wu et al., 2021a, 2021b). In recent years, Miscellaneous innovative applications of narirutin was also supported the further study of its pharmacological effects. By using Silico, it was shown that citrus flavone myoglobin interacts significantly with most of the receptors and possesses a good inhibitory activity *in vitro*, indicating its powerful role in the management of diabetes and its complications (Qurtam et al., 2021). The polymerized nanoparticles were suitable for delivering the flavonoid naringin to the gut, avoiding gastric degradation and improving its bioavailability from oral solid dosage forms, as was the case with other flavonoids such as narirutin (Mohanty et al., 2021).

After oral administration, a series of biological transformation reactions will occur until the drug is eliminated from the body, accompanied by the therapeutic efficacy or toxic side-effect, which provides a pivotal theoretical basis for *in vivo* mechanisms exploitation of drugs (Wu et al., 2021a, 2021b). Previous studies mostly focused on the pharmacological activity of naringin at present, rather few on narirutin metabolites mining. That is to say, an in-depth study on narirutin metabolic pathways *in vivo* and *in vivo* carried out was of great importance. Therefore, it is important to establish an accurate and high-resolution qualitative analysis method for the comprehensive characterization of narirutin metabolites.

Xenobiotic metabolism is a natural reaction to the ubiquity of exotic compounds. However, they are usually metabolized into different forms by different metabolic pathways (Shang et al., 2017). Because of its little amount, the metabolite signal is usually masked by the background noise produced by endogenous substances. In recent years, with the continuous develop-

ment of liquid chromatography mass spectrometry (LC-MS), its performances of rapid detection speed, high sensitivity and high resolution have already been improved. Therefore, LC-MS has been frequently used to clarify the separation and analysis of drug metabolites (Jiang et al., 2021; Lan et al., 2022). Especially, ultra-high performance liquid chromatography quadrupole exactive Orbitrap MS/MS (UPLC-Q-Exactive Orbitrap MS/MS) method was established to screen and identify the naringin metabolites. In our study, we proposed a strategy named “Analogous Core Recursion” (ACR), which combined with the “Diagnostic Fragment Ion Clusters” (DFICs) and “Characteristic Suggestive Ions” (CSIs) obtained by our recursive analysis, for the inference and recognition of narirutin metabolites to improve the efficiency of metabolite recognition. Finally, based on these detected metabolites, the metabolic pathways of narirutin were also proposed so as to provide the basis for the biological activity study.

## 2. Material and methods

### 2.1. Chemicals and reagents

Narirutin (MUST-20111105, its physical and chemical properties were shown in Table 1) was purchased from Chengdu Must Bio-technology Co., Ltd (Sichuan, China). The reference standard with purity higher than 99% was applicable to HPLC analysis. Pooled male Sprague Dawley (SD) rat liver microsomes (20210305, 1 mL, 20 mg/mL),  $\beta$ -nicotinamide adenine dinucleotide phosphate (NADPH), uridine 5'-diphosphoglucuronic acid trisodium salt (UDPGA) and Magnesium chloride ( $MgCl_2$ ) were purchased from NEWGAINBIO Co., Ltd (Wuxi, China). UHPLC grade acetonitrile, methanol and formic acid (FA) were purchased from Thermo Fisher Scientific (Fair Lawn, NJ, USA), and pure water for analysis was bought from Watson Group Co., Ltd (Guangzhou, China). All the other chemicals of analytical grade were available at the work station, Shandong Academy of Chinese Medicine (Jinan, China). Grace Pure<sup>®</sup>SPE C<sub>18</sub>-Low solid phase extraction cartridges (200 mg/3 mL, 59 mm, 70 Å) were purchased from Grace Davison Discovery Science (Deerfield, IL, USA).

### 2.2. Animals and drug administration

Six male SD rats weighting  $200 \pm 10$  g were obtained from Jinan Pengyue Experimental Animal Breeding Co., Ltd (Shandong, China). The rats were housed in a controlled room at standard temperature ( $24 \pm 2$  °C) and humidity ( $70 \pm 5\%$ ) and kept on a 12 h light/12 h dark regime. After a week of acclimation, the rats were randomly divided into two groups:

**Table 1** The physicochemical properties of narirutin.

Property Name	Property Value
density	1.7 ± 0.1 g/cm <sup>3</sup>
Boiling point	924.3 ± 65.0 °C at 760 mmHg
melting point	152–190 °C
Molecular Formula	C <sub>27</sub> H <sub>32</sub> O <sub>14</sub>
Molecular Weight	580.5
Exact Mass	580.17920569
Appearance trait	Grey powder
Vapor pressure	0.0 ± 0.3 mmHg at 25 °C
flash point	307.3 ± 27.8 °C
Refractive index	1.708
XLogP3-AA	-1.1
Hydrogen Bond Donor Count	8
Hydrogen Bond Acceptor Count	14
Rotatable Bond Count	6
Topological Polar Surface Area	225 Å <sup>2</sup>
Heavy Atom Count	41

Drug Group (n = 3) and Control Group (n = 3) for testing plasma, urine and faeces individually. They were fasted for 12 h with free access to water prior to the experiment. Narirutin dissolved in normal saline was orally given to the rats in Drug Group were at a dose of 150 mg/kg body weight. Rats in Control Group were given the same volume of normal saline. All the rats were administered for three consecutive days and fed in animal room of Shandong International Biotechnology Park. The animal protocols were approved by the institutional Animal Care and Use Committee at Binzhou Medical University (2021-085). The animal facilities and protocols were complied with the Guide for the Care and Use of Laboratory Animals (USA National Research Council, 1996).

### 2.3. Sample collection and preparation

#### 2.3.1. Preparation of *in vivo* samples

Blood samples (0.5 mL) were taken from the suborbital venous plexus of rats at 0.5, 1, 1.5, 2, 4, and 6 h post-administration. Each sample was centrifuged at 3,500 rpm for 10 min to separate plasma samples and preserved in three parts. Urine and faeces samples were collected 0–24 h after oral administration. Rat liver tissues were collected 24 h after the last administration. All the homogeneous biological samples from the same group were merged into a collective sample.

Three copies of plasma samples were treated in three ways. Randomly select any two samples, and methanol or acetonitrile was added to the blood samples at a ratio of 1:3 respectively. Each sample was centrifuged at 3,500 rpm for 10 min to separate supernatant liquid. Another sample of blood plasma (1 mL) were added to solid phase extraction (SPE) cartridges pretreated with methanol (5 mL) and deionized water (5 mL), respectively. Then, the SPE cartridges were successively washed with deionized water (3 mL) and methanol (3 mL).

Urine samples were centrifuged at 12,000 rpm for 15 min to collect supernatant. Rat faeces samples were lyophilized, ground and mixed evenly. Then pure water (10 mL) was added into the excrement powder (2 g) for ultrasonic treatment for 0.5 h and the suspension was centrifuged at 3,500 rpm for

15 min to obtain the supernatant. The rat liver tissues were ground with normal saline and centrifuged at 3,500 rpm for 15 min to obtain the supernatant liquid. The treated urine, faeces and liver tissues samples were passed through SPE cartridges and methanol eluent was collected to use for the further instrumental analysis.

#### 2.3.2. Preparation of *in vitro* samples

In the incubation system containing MyCl<sub>2</sub> (3 mM), liver microsomes (20 mg/mL) and narirutin (0.1 mg/mL), incubated for 5 min at 37 °C. NADPH solution (25 mg/mL) was added to start the reaction and incubated for 4 h. The total incubation amount in the system was 1 mL. At 5, 10, 15, 30, 45, 60, 120 and 240 min, 100 µL of system solution was taken and 200 µL of cold acetonitrile was added to stop the reaction. The solution at each stage was mixed and centrifuged at 3,500 rpm for 15 min to take the supernatant.

#### 2.3.3. Sample preservation and pre-injection treatment

After all the samples were prepared, the organic solvent was blow-dried with N<sub>2</sub> at room temperature. The samples were redissolved with 300 µL methanol, centrifuged at 14,000 rpm for 10 min at high speed. The supernatant was taken in liquid sample bottle for the subsequent instrumental analysis.

### 2.4. Instruments and analytical conditions

UHPLC analysis was performed on a DIONEX Ultimate 3000 UHPLC system (Thermo Fisher Scientific, MA, USA), which equipped with a binary pump, an automated sampler and a column compartment. The chromatographic separations were performed on Waters ACQUITY BEH C<sub>18</sub> column (2.1 × 100 mm, 1.7 µm). HRMS and MS/MS spectra were obtained using a Q-Exactive Orbitrap mass spectrometer.

The mobile phase consisted of 0.1% formic acid aqueous solution (A) and acetonitrile (B) at a flow rate of 0.3 mL/min. The linear gradient procedure was described as follows: 0–5 min, 5%–30%B; 5–10 min, 30%–50%B; 10–27 min, 50%–90%B; 27–30 min, 90%–5%B. The injection volume was 2 µL. An analytical run was performed by mass spectrometry in positive and negative ion modes. The ion source parameters were listed as follows: nitrogen (purity ≥ 99.99%) served as the sheath gas and auxiliary gas. The flow of sheath gas (nitrogen) was 45 arb and auxiliary gas (nitrogen) was 10 arb. A capillary temperature of 320 °C, probe heater temperature of 320 °C and spray voltage of 3,800/3,500 V (+/-) were used. Orbitrap analyzers obtained high-resolution mass spectra with a full scan in *m/z* 80 ~ 1,200 mass range at a resolution of 70,000 in MS and a resolution of 17,500 in dd MS/MS.

### 2.5. Peak selections and data processing

A Thermo Xcalibur 2.1 workstation was used for the data acquisition and processing. To obtain as many ESI-MS/MS fragment ions of narirutin metabolites as possible, the base peak ions detected with an intensity over 40,000 in positive ion mode and 10,000 in negative ion mode were selected for chemical identification. The chemical formulas attributed to the selected peaks were calculated using a formula predictor by setting the parameters as follows: C [5–30], H [5–60], O

[1–20], S [0–5], N [0–5] and the ring double bond (RDB) equivalent value [3–20].

### 3. Results

#### 3.1. Establishment of analytical strategy

It is important to establish an efficient analytical strategy to capture the signals of narirutin metabolites. Therefore, in this study, an analytical strategy based on ACR was proposed to screen and identify narirutin metabolites using complex mass spectra information. In the analysis strategy, based on the core structure of a large class of substances, a single compound was deduced, and according to the DFICs and CSIs, the metabolites and the possible sites of their metabolic reactions were determined (Fig. 1). Firstly, according to the cleavage mode of the basic core structure of flavonoids, the cleavage rules of narirutin were deduced by mass spectra, and the DFICs of narirutin were identified by combining the secondary mass spectra information of narirutin. Secondly, based on the metabolic characteristics of compounds *in vivo*, the potential phase II metabolic reactions, such as deglycosylation to aglycone, glucuronidation and sulfation, were predicted. Correspondingly, the DFICs were determined based on the abovementioned metabolites. Thirdly, based on the DFICs obtained in the previous two steps, the metabolites were further speculated. Fourthly, the possible sites of metabolic reactions, such as the A ring, B ring and sugar group, were deduced by indicating the distinction of CSIs. Considering the retention time of metabolites and the corresponding ClogP value, isomers were preliminarily distinguished. Finally, the accuracy and reliability of the analysis strategy were verified by comparison to the fragmentation cleavage behavior of the reference substance and metabolites of narirutin.

ability of the analysis strategy were verified by comparison to the fragmentation cleavage behavior of the reference substance and metabolites of narirutin.

#### 3.2. Interpretation of the narirutin metabolites analysis strategy

There are two basic cleavage methods of flavonoids in mass spectrometry. The first method is the Retro-Diels-Alder (RDA) cleavage that produces 2 ions at  $m/z$  120 and  $m/z$  102, and the second method yields a fragment ion at  $m/z$  105. The three fragment ions produced by these methods are derived from the core structure at  $m/z$  222. CO can be easily removed from the ion at  $m/z$  105 to produce the ion at  $m/z$  77. The aglycone of narirutin is a dihydroflavonoid, which has 3 more Os (2 in the A ring and 1 in the B ring) and 2 more Hs (C2-C3) than the nuclear structure of the basic flavone. Thus, we speculated that the above two cleavage methods were applicable to narirutin. Based on the above cleavage rules, we recursed the DFICs of narirutin as  $m/z$  580,  $m/z$  272,  $m/z$  152,  $m/z$  120 and  $m/z$  94 (Fig. 2). The corresponding fragment ions in different ion modes were as follows:  $m/z$  579,  $m/z$  271,  $m/z$  151,  $m/z$  119 and  $m/z$  93 in the negative ion mode; and  $m/z$  581,  $m/z$  273,  $m/z$  153,  $m/z$  121 and  $m/z$  95 in the positive ion mode. By comparing the information of the narirutin standard in electron spray ionization (ESI)-MS/MS (Fig. 3 and Fig. 4), the correctness of the DFICs obtained by recursive analysis were confirmed, implying a further analysis could be employed.

Narirutin is produced by combining the rutinose group at the C7 position on naringenin. The polarity of narirutin is relatively large, and the glucuronidation, sulfation and other

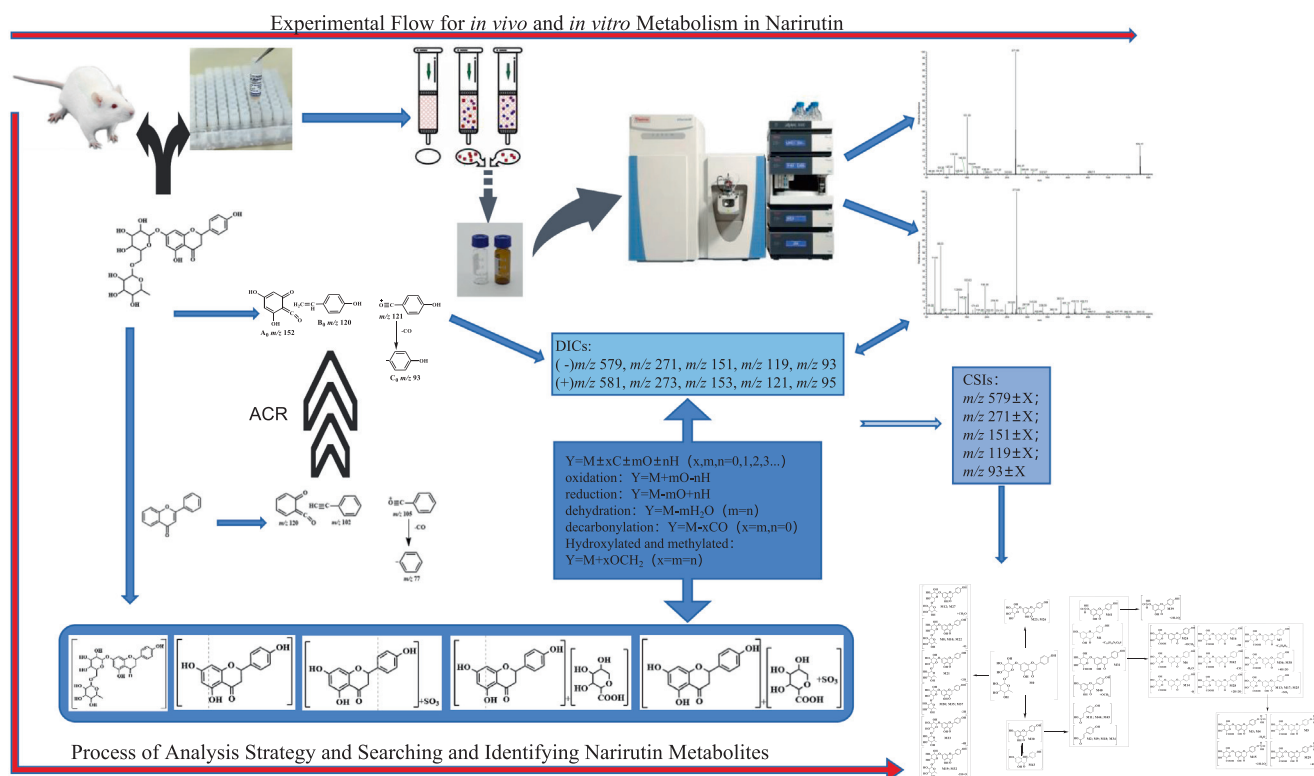


Fig 1 Schematic diagram of analysis strategies and the experimental processes of Narirutin metabolism *in vitro* and *in vivo*.

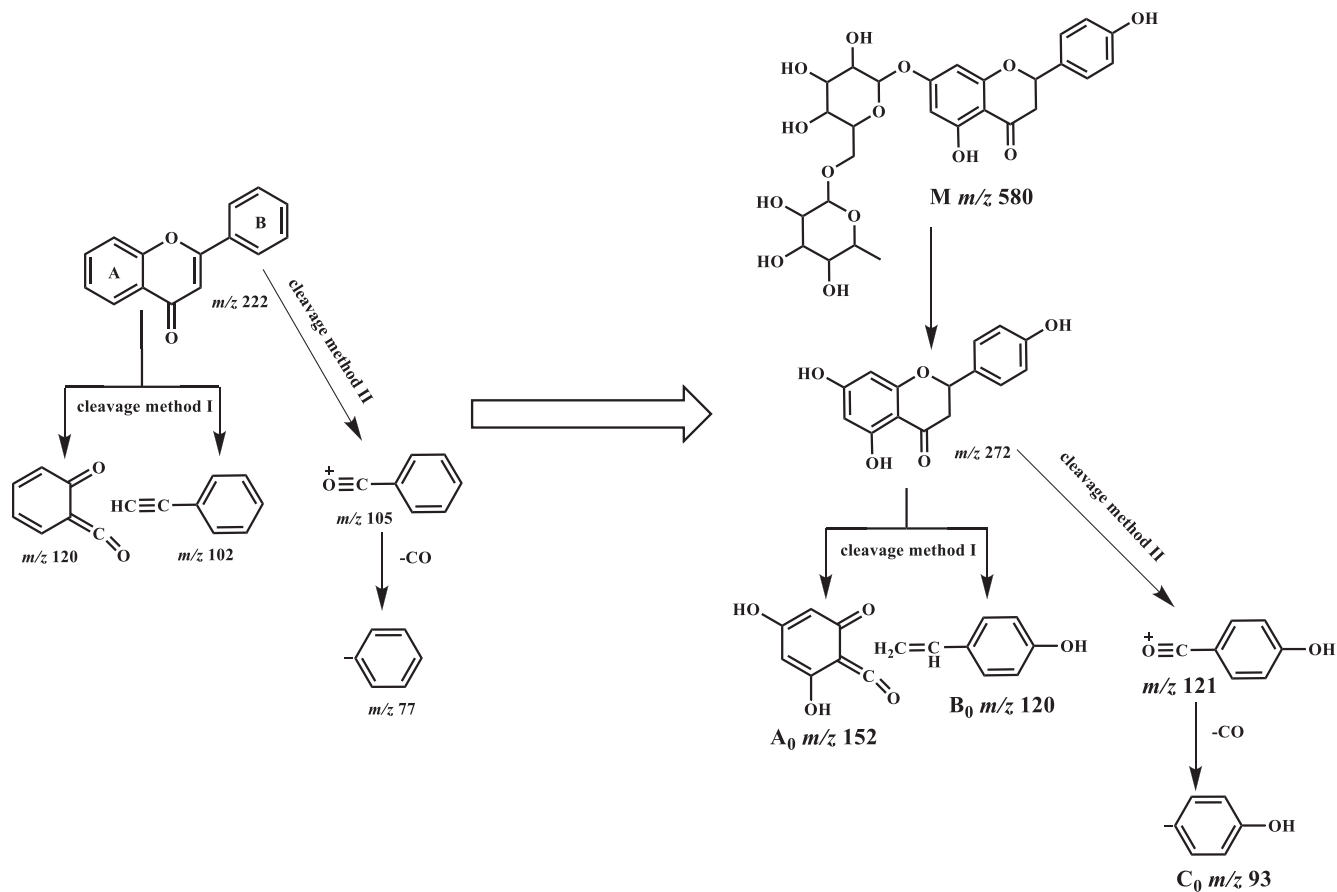


Fig 2 Cleavage of core structure of flavonoids and Narirutin.

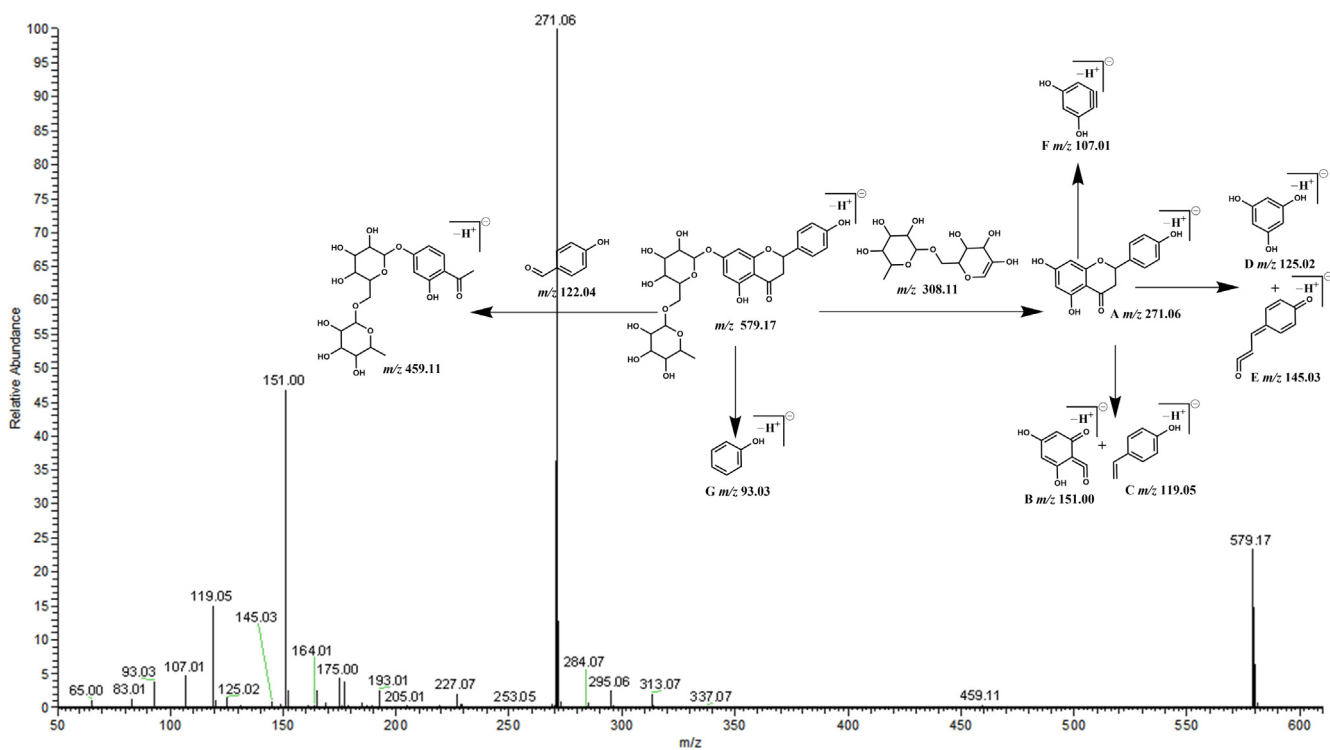


Fig. 3 Secondary mass spectrum and cleavage rule in negative mode.

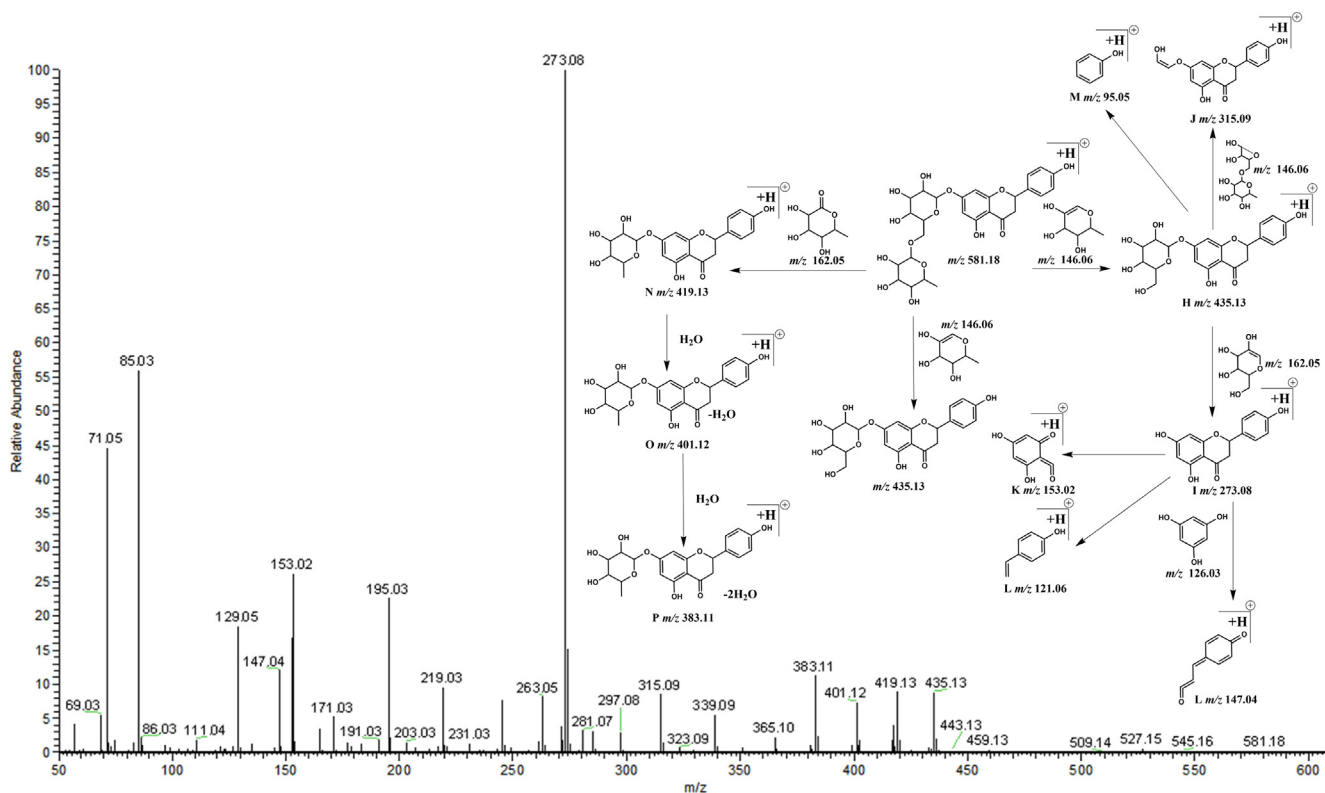


Fig. 4 Secondary mass spectrum and cleavage rule in positive mode.

binding reactions with narirutin are difficult due to the steric hindrance of the rutinosyl group. However, the polarity of naringenin produced by metabolism is low, which is not conducive to excretion by the body. Because naringenin has little steric hindrance, it is speculated that glucuronidation, sulfation and other reactions may occur in naringenin aglycone. Fragment ions, such as  $m/z$  176,  $m/z$  114 and  $m/z$  80, can be generated by the glucuronic acid group and sulfate group, thus enriching their DFICs. For example, in the negative ion mode, the DFICs produced by naringenin glucuronic acid were  $m/z$  447,  $m/z$  271,  $m/z$  176,  $m/z$  151,  $m/z$  119,  $m/z$  114 and  $m/z$  93, and the DFICs formed by naringenin sulfate were  $m/z$  351,  $m/z$  271,  $m/z$  151,  $m/z$  119,  $m/z$  93 and  $m/z$  79.

According to the DFICs of the corresponding compounds and the secondary mass spectra information of different samples, the metabolites obtained by oxidation, reduction and dehydration reactions were predicted. In the present study, we proposed the following recursive formula:  $Y = M \pm xC \pm mO \pm nH$ ; where  $Y$  is the exact molecular weight of the metabolite;  $M$  is the exact molecular weight of the prototype compound;  $C$ ,  $O$  and  $H$  represent the exact molecular weights of carbon, oxygen and hydrogen, respectively; and  $x$ ,  $m$  and  $n$  are integers  $\geq 0$ . According to different types of metabolic reactions, such as oxidation, reduction and dehydration, different  $x$ ,  $m$  and  $n$  values were substituted into the formula, and the obtained  $Y$  values were searched in the corresponding MS/MS spectra, which allowed a preliminary prediction of the metabolites (Fig. 1).

The regular changes in DFICs indicated where metabolic reactions were likely to occur. Taking narirutin as an example,

the following DFICs changes were estimated in negative ion mode: if the metabolic reactions occurred in the A ring, the DFICs changes were  $579 \pm X$ ,  $m/z$  271  $\pm X$ ,  $m/z$  151  $\pm X$ ,  $m/z$  119 and  $m/z$  93; if the reaction occurred in the B ring, the DFICs changes were  $m/z$  579  $\pm X$ ,  $m/z$  271  $\pm X$ ,  $m/z$  151,  $m/z$  119  $\pm X$  and  $m/z$  93  $\pm X$ ; and if the reaction occurred at the relatively rare rutinosyl group, the DFICs changes were  $m/z$  579  $\pm X$ ,  $m/z$  271,  $m/z$  151,  $m/z$  119 and  $m/z$  93. Furthermore, the retention time of the metabolites and their corresponding Clog $P$  values were combined to preliminarily distinguish and identify the isomers produced by the same reaction at different sites.

### 3.3. Identification and structural elucidation of narirutin metabolites

A total of 46 narirutin metabolites (narirutin included) were detected and identified in the plasma, urine, faeces, liver tissues and liver microsomes of SD rats using ultra-high performance liquid chromatography quadrupole exactive orbitrap MS/MS (UHPLC-Q-Exactive Orbitrap MS/MS). Among them, 22, 12, 4 and 19 metabolites were identified in plasma, urine, liver and liver microsomes, respectively. However, no metabolites were identified in rat faeces. The relative content of each metabolite was estimated according to the intensity and peak area information of the MS/MS spectra. The LC-MS data of these detected metabolites were summarized in Table 2 and Fig. 5, and the extracted ion chromatogram (EIC) profiles of the metabolites in the different samples are illustrated in Fig. 6.

**Table 2** Summary of narirutin metabolites in rats.

Peak	Ion Mode	tR/ min	Formula	Theoretical Mass m/z	Experimental Mass m/z	RDB	Error (ppm)	MS/MS fragment ions	PS	PM	PA	U	L	LM	Relative content
<b>M0</b>	N	5.92	C <sub>27</sub> H <sub>32</sub> O <sub>14</sub>	579.17193	579.1701	12.5	-1.264	579.17(24.92),459.11(0.39),271.06(100.00),165.02(2.65),151.00(46.95),145.03(0.94),125.02(1.48),119.05(15.62),107.01(4.76),93.03(4.17)	✓	✓	✓	✓	✓	✓	++ , ##
	P	5.92	C <sub>27</sub> H <sub>32</sub> O <sub>14</sub>	581.18648	581.18591	11.5	-0.984	581.18(0.14),435.13(8.64),419.13(9.16),383.11(10.94),365.10(2.29),339.09(5.77),315.09(8.65),273.08(100.00),219.03(9.55),153.02(26.21),147.04(11.73)	✓	✓	✓	✓	✓	✓	
<b>M1</b>	N	3.15	C <sub>25</sub> H <sub>27</sub> N <sub>3</sub> SO <sub>11</sub>	576.12935	576.13464	14.5	1.081	576.13(100.00),447.09(11.33),400.10(26.57),271.06(35.68),151.00(11.87),119.05(9.11),74.02(2.58),59.01(8.09)				✓			+
<b>M2</b>	N	3.73	C <sub>9</sub> H <sub>8</sub> O <sub>3</sub>	163.04007	163.03856	6.5	-2.518	163.04(10.72),119.05(100.00)					✓		++
<b>M3</b>	N	3.91	C <sub>21</sub> H <sub>18</sub> SO <sub>13</sub>	509.03953	509.0387	13.5	0.515	509.04(88.50),333.01(35.45),253.05(100.00),113.02(5.24),79.96(6.51)			✓				+
<b>M4</b>	N	4.26	C <sub>21</sub> H <sub>18</sub> SO <sub>13</sub>	509.03953	509.03888	13.5	0.869	509.04(70.15),333.01(32.98),253.05(100.00),113.02(5.87),79.96(6.98)	✓						+
<b>M5</b>	N	4.64	C <sub>21</sub> H <sub>18</sub> SO <sub>14</sub>	525.03445	525.03381	13.5	0.872	525.03(51.96),445.08(0.87),349.00(18.81),269.04(100.00),113.02(3.45),79.96(1.57)			✓				+
<b>M6</b>	N	4.73	C <sub>21</sub> H <sub>18</sub> O <sub>10</sub>	429.08272	429.082	13.5	0.878	429.08(8.48),253.05(100.00),175.02(20.30),113.02(44.19)	✓	✓	✓				+
<b>M7</b>	N	4.79	C <sub>27</sub> H <sub>28</sub> O <sub>17</sub>	623.12537	623.12463	14.5	0.569	623.12(29.33),447.09(100.00),271.06(63.91),175.02(15.05),151.00(27.95),119.05(6.65),113.02(53.95),93.03(2.86)				✓			++
<b>M8</b>	N	4.98	C <sub>27</sub> H <sub>32</sub> O <sub>15</sub>	595.16684	595.16571	12.5	-0.061	595.17(55.57),459.11(1.16),287.06(30.79),151.00(5.25),135.04(2.87),125.02(100.00)						✓	#
<b>M9</b>	N	5.09	C <sub>9</sub> H <sub>8</sub> O <sub>3</sub>	163.04007	163.03873	6.5	-1.476	163.04(10.38),119.05(100.00)					✓		++
<b>M10</b>	N	5.34	C <sub>27</sub> H <sub>32</sub> O <sub>15</sub>	595.16684	595.16602	12.5	0.459	595.17(30.09),459.11(1.26),287.06(62.78),193.01(1.99),151.00(100.00),135.04(34.60),125.02(4.07)						✓	##
	P	5.35	C <sub>27</sub> H <sub>32</sub> O <sub>15</sub>	597.1814	597.18048	11.5	-1.535	435.13(8.05),399.10(10.55),331.08(8.65),289.07(100.00),219.03(10.68),195.03(24.71),153.02(25.86),129.05(20.59)						✓	
<b>M11</b>	N	5.40	C <sub>9</sub> H <sub>10</sub> O <sub>3</sub>	165.05572	165.05441	5.5	-1.276	165.05(35.83),147.04(100.00),121.06(17.99),119.05(33.73),93.03(4.53)	✓	✓			✓		++
<b>M12</b>	N	5.45	C <sub>28</sub> H <sub>34</sub> O <sub>15</sub>	609.18249	609.18152	12.5	0.203	609.18(25.63),301.07(14.78),283.06(66.06),271.06(3.27),119.05(29.82),93.03(1.50)						✓	#
<b>M13</b>	N	5.51	C <sub>21</sub> H <sub>20</sub> SO <sub>14</sub>	527.0501	527.04956	12.5	1.058	527.05(57.55),447.09(31.97),351.02(53.62),271.06(100.00),175.02(8.07),151.00(16.50),119.05(4.43),113.02(46.33)			✓				+
<b>M14</b>	N	5.59	C <sub>21</sub> H <sub>20</sub> O <sub>10</sub>	431.09837	431.09763	12.5	0.828	431.10(100.00),255.06(43.96),175.02(24.69),149.02(36.27),113.02(66.42)	✓						+
<b>M15</b>	N	5.63	C <sub>21</sub> H <sub>22</sub> SO <sub>12</sub>	497.07592	497.07568	11.5	1.724	497.08(40.71),321.04(100.00),241.09(23.22),175.02(2.80),135.04(2.90),121.03(12.76),119.05(3.92),113.02(17.38),79.96(8.68)	✓						++
<b>M16</b>	P	5.70	C <sub>21</sub> H <sub>18</sub> O <sub>11</sub>	447.09219	447.09164	12.5	-1.225	447.09(9.04),271.06(100.00),153.02(1.38)	✓	✓	✓				+
<b>M17</b>	N	5.74	C <sub>21</sub> H <sub>20</sub> SO <sub>14</sub>	527.0501	527.0495	12.5	0.944	527.05(41.57),447.09(22.43),351.02(61.38),271.06(100.00),175.02(8.35),151.00(36.49),119.05(6.89),113.02(44.47),93.03(3.02)				✓			++
	N	5.83	C <sub>9</sub> H <sub>8</sub> O <sub>3</sub>	163.04007	163.03879	6.5	-1.108	163.04(26.90),119.05(100.00),93.03(1.39)					✓		++
<b>M19</b>	P	5.88	C <sub>27</sub> H <sub>30</sub> O <sub>15</sub>	595.16575	595.16339	12.5	-3.959	595.16(1.87),287.05(100.00),165.02(7.84),129.05(6.04)						✓	#
<b>M20</b>	N	5.88	C <sub>27</sub> H <sub>30</sub> O <sub>14</sub>	577.15628	577.15515	13.5	-0.055	577.15(14.10),269.04(100.00),151.00(5.80),119.05(2.08),93.03(0.68)						✓	##

(continued on next page)

**Table 2** (continued)

Peak	Ion Mode	tR/min	Formula	Theoretical Mass m/z	Experimental Mass m/z	RDB	Error (ppm)	MS/MS fragment ions	PS	PM	PA	U	L	LM	Relative content
	P	5.89	C <sub>27</sub> H <sub>30</sub> O <sub>14</sub>	579.17083	579.17004	12.5	-1.367	579.17(3.31), 433.11(27.34), 271.06(100.00), 153.02(0.65), 129.05(1.34)							✓
<b>M21</b>	N	5.90	C <sub>27</sub> H <sub>32</sub> O <sub>16</sub>	611.16176	611.1601	12.5	-0.918	611.16(100.00), 489.12(9.34), 303.05(78.48), 285.04(78.12), 269.04(40.10), 151.00(82.42), 125.02(58.54), 119.05(22.81)							✓ #
<b>M22</b>	N	5.91	C <sub>27</sub> H <sub>32</sub> O <sub>15</sub>	595.16684	595.16382	12.5	-3.237	595.17(63.48), 287.06(100.00), 151.00(73.86), 135.04(22.98), 125.02(12.72)							✓ #
<b>M23</b>	N	6.01	C <sub>21</sub> H <sub>22</sub> O <sub>10</sub>	433.11402	433.11301	11.5	0.2	433.11(2.90), 271.06(100.00), 151.00(37.10), 119.05(12.49), 93.03(5.76)							✓ #
<b>M24</b>	P	6.05	C <sub>22</sub> H <sub>22</sub> O <sub>12</sub>	479.1184	479.11768	11.5	-1.508	479.11(8.06), 303.09(100.00), 183.03(44.06), 147.04(13.68), 136.06(24.43)							✓ #
<b>M25</b>	N	6.13	C <sub>21</sub> H <sub>20</sub> SO <sub>14</sub>	527.0501	527.0498	12.5	1.514	527.05(71.79), 447.09(35.27), 351.02(60.23), 271.06(100.00), 175.02(8.04), 151.00(30.95), 119.05(7.35), 113.02(52.87)	✓						+
<b>M26</b>	N	6.24	C <sub>21</sub> H <sub>22</sub> O <sub>10</sub>	433.11402	433.11319	11.5	0.616	433.11(4.76), 271.06(100.00), 151.00(32.20), 119.05(12.93), 93.03(4.14)							✓ #
<b>M27</b>	N	6.26	C <sub>28</sub> H <sub>34</sub> O <sub>15</sub>	609.18249	609.1814	12.5	0.006	609.18(21.56), 301.07(100.00), 271.06(1.54), 151.00(5.09), 149.06(1.18), 125.02(4.11)							✓ #
<b>M28</b>	N	6.26	C <sub>21</sub> H <sub>22</sub> O <sub>9</sub>	417.11911	417.11862	11.5	1.466	417.12(71.42), 241.09(27.61), 175.02(35.26), 135.04(13.45), 121.03(37.58), 119.05(20.25), 113.02(100.00), 93.03(3.63)	✓	✓	✓	✓			++
<b>M29</b>	N	6.27	C <sub>21</sub> H <sub>24</sub> SO <sub>13</sub>	515.08648	515.0838	10.5	-3.083	515.08(4.97), 271.06(23.08), 151.00(52.48), 119.05(6.10), 79.96(3.93)	✓	✓		✓			++
<b>M30</b>	P	6.34	C <sub>15</sub> H <sub>12</sub> O <sub>5</sub>	273.07575	273.07535	9.5	-1.465	273.08(82.96), 171.03(22.67), 153.02(100.00), 147.04(47.75), 119.05(5.95)	✓		✓				✓ ++, #
	N	6.35	C <sub>15</sub> H <sub>12</sub> O <sub>5</sub>	271.06065	271.06	10.5	-0.369	271.06(99.44), 151.00(100.00), 119.05(56.96), 93.03(9.99)	✓		✓				✓
<b>M31</b>	N	6.35	C <sub>21</sub> H <sub>20</sub> O <sub>11</sub>	447.09328	447.09244	12.5	0.564	447.09(93.15), 271.06(100.00), 175.02(52.06), 151.00(72.00), 119.05(23.58), 113.02(61.28), 93.03(4.61)			✓				✓ ++, #
<b>M32</b>	P	6.46	C <sub>27</sub> H <sub>30</sub> O <sub>15</sub>	595.16575	595.16473	12.5	-1.708	595.16(1.36), 577.16(3.62), 435.13(2.36), 273.07(100.00), 171.03(16.80), 153.02(35.66), 147.04(10.78)							✓ #
<b>M33</b>	N	6.46	C <sub>27</sub> H <sub>28</sub> O <sub>14</sub>	575.14063	575.13977	14.5	0.414	575.14(17.85), 433.11(6.95), 271.06(100.00), 151.00(30.86), 119.05(9.39), 93.03(3.14)							✓ #
<b>M34</b>	N	6.47	C <sub>9</sub> H <sub>8</sub> O <sub>3</sub>	163.04007	163.03859	6.5	-2.334	163.04(3.36), 119.05(100.00)					✓		++
<b>M35</b>	P	6.50	C <sub>27</sub> H <sub>30</sub> O <sub>14</sub>	579.17083	579.1698	12.5	-1.782	435.13(8.86), 273.07(100.00), 195.03(4.15), 171.03(21.15), 153.02(41.65)							✓ #
<b>M36</b>	N	6.57	C <sub>21</sub> H <sub>24</sub> O <sub>9</sub>	419.13476	419.13397	10.5	0.743	419.13(100.00), 243.10(36.31), 175.02(9.64), 123.04(6.62), 121.03(2.99), 119.05(3.35), 113.02(40.21), 93.03(3.35)	✓		✓				+
<b>M37</b>	N	6.84	C <sub>27</sub> H <sub>30</sub> O <sub>14</sub>	577.15628	577.15546	13.5	0.482	433.11(12.63), 271.06(100.00), 151.00(34.73), 119.05(14.84), 93.03(4.07)							✓ #
	P	6.84	C <sub>27</sub> H <sub>30</sub> O <sub>14</sub>	579.17083	579.16992	12.5	-1.575	579.17(1.49), 417.12(2.76), 273.07(100.00), 171.03(21.48), 153.02(43.29)							✓
<b>M38</b>	N	7.03	C <sub>21</sub> H <sub>24</sub> O <sub>9</sub>	419.13476	419.13419	10.5	1.268	419.13(100.00), 243.10(46.94), 175.02(16.80), 123.04(7.29), 121.03(3.79), 119.05(2.31), 113.02(57.02), 93.03(2.26)	✓		✓				+
<b>M39</b>	N	7.06	C <sub>15</sub> H <sub>14</sub> SO <sub>6</sub>	321.04383	321.0433	9.5	1.759	321.04(100.00), 241.09(36.73), 121.03(52.72), 119.05(23.94), 93.03(3.41), 79.96(23.50)	✓	✓	✓				++
<b>M40</b>	N	7.14	C <sub>16</sub> H <sub>14</sub> O <sub>6</sub>	301.07176	301.07104	10.5	1.247	301.07(100.00), 271.06(10.68), 181.05(4.07), 119.05(48.24), 93.03(20.67)				✓			++

Table 2 (continued)

Peak	Ion Mode	tR/min	Formula	Theoretical Mass m/z	Experimental Mass m/z	RDB	Error (ppm)	MS/MS fragment ions	PS	PM	PA	U	L	LM	Relative content
<b>M41</b>	N	7.40	C <sub>15</sub> H <sub>12</sub> SO <sub>8</sub>	351.01801	351.01727	10.5	1.013	351.02(30.68), 271.06(100.00), 151.00(37.10), 119.05(10.93), 93.03(5.37), 79.96(7.72)	✓	✓	✓				+
<b>M42</b>	P	7.83	C <sub>20</sub> H <sub>20</sub> O <sub>10</sub>	421.11292	421.10986	10.5	-7.274	421.11(79.21), 403.25(2.22), 245.05(100.00), 121.03(6.56)			✓				++
<b>M43</b>	N	8.49	C <sub>15</sub> H <sub>12</sub> O <sub>5</sub>	271.06065	271.06094	10.5	3.099	271.06(100.00), 151.00(83.81), 119.05(59.18), 93.03(13.77)	✓		✓		✓		++
	P	8.5	C <sub>15</sub> H <sub>12</sub> O <sub>5</sub>	273.07575	273.07541	9.5	-1.245	273.08(100.00), 171.03(4.27), 153.02(99.87), 147.04(57.23), 119.05(7.63)	✓	✓	✓		✓		+++
<b>M44</b>	N	9.89	C <sub>9</sub> H <sub>10</sub> O <sub>3</sub>	165.05572	165.0544	5.5	-1.337	165.05(48.70), 147.04(14.57), 121.06(100.00), 119.05(10.41), 93.03(6.33)	✓				✓		++
<b>M45</b>	N	10.73	C <sub>9</sub> H <sub>10</sub> O <sub>3</sub>	165.05572	165.05435	5.5	-1.64	165.05(55.67), 147.04(26.20), 121.06(100.00), 119.05(11.15), 93.03(8.98)	✓				✓		++

PS: plasma SPE extraction; PM: plasma methanol precipitation; PA: plasma acetonitrile precipitation; U: urine SPE extraction; LS: liver SPE extraction; LM: Prototype drug liver microsomal treatment; detected: + (*in vivo*), # (*in vitro*); abundant: ++ (*in vivo*), ## (*in vitro*).

### 3.3.1. Identification of narirutin metabolites

The primary metabolite of naringin was mainly obtained from liver microsomes *in vitro*. Only the metabolites of narirutin deglycosylation and aglycone glucuronic acid were identified *in vitro* and *in vivo*, and there was an obvious difference of *in vitro* and *in vivo* metabolites. In addition to using the changes of CSIs, the metabolites were identified using DFICs at  $m/z$  579,  $m/z$  271,  $m/z$  151,  $m/z$  119 and  $m/z$  93 in negative ion mode as well as at  $m/z$  581,  $m/z$  273,  $m/z$  153,  $m/z$  121 and  $m/z$  95 in positive ion mode.

**M30** and **M43** were 308 Da less massive than narirutin, suggesting that they may be products of narirutin lacking the ruti-noside group. Based on the DFICs, we found that **M30** and **M43** possessed the same theoretical  $[M + H]^+ / [M - H]^-$  ions at  $m/z$  273.07575 (C<sub>15</sub>H<sub>11</sub>O<sub>5</sub>, mass error  $\leq 3$  ppm) in the positive ion mode as well as at  $m/z$  271.06065 (C<sub>15</sub>H<sub>13</sub>O<sub>5</sub>, mass error  $\leq 3$  ppm) in the negative ion mode. In the ESI-MS/MS spectra of **M30** and **M43**, a series of diagnostic ions for naringin were observed, including  $m/z$  151.00,  $m/z$  119.05 and  $m/z$  93.03 in the negative ion mode as well as  $m/z$  153.02,  $m/z$  121.06 and  $m/z$  95.05 in the positive ion mode, which provided evidence that **M30** and **M43** were naringin and its isomer. Dihydroflavone and its corresponding chalcone were isomers of each other. Chalcone is a planar molecule, and its hydrophobicity is stronger than the corresponding dihydroflavone, resulting in a larger ClogP value. In reversed-phase separation mode, compounds with a higher ClogP value generally exhibit longer retention times. Thus, **M30** was identified as naringenin, and **M43** was identified as naringenin chalcone.

In the negative ion mode, the same base peak ions at  $m/z$  433.11402 ( $[M - H - C_6H_{12}O_4]^-$ ) and some other DFICs at  $m/z$  151.00,  $m/z$  119.05 and  $m/z$  93.03 were present in the **M23** and **M26** metabolites. Glucose-binding sites were determined by comparing the retention time and ClogP value of glucose-binding hydroxyl groups at different positions of naringenin. The retention times of **M23** and **M26** were relatively similar and were between those of naringenin aglycone and narirutin. Therefore, **M23** and **M26** were deduced as 7-glucose-naringin and 4'-glucose-naringin, respectively.

Through the DFICs and the changes of CSIs, we speculated that some metabolites, such as **M8**, **M10**, **M12**, **M19**, **M20**, **M21**, **M22**, **M27**, **M32**, **M33**, **M35** and **M37**, were obtained by oxidation, hydroxylation and other reactions. The oxidation reaction is a type of chemical reaction that easily occurs in the body via many mechanisms, including increased oxygen oxidation, increased dehydrogenation and increased coexistence of oxygen and dehydrogenation.

**M8**, **M10** and **M22** gave rise to the  $[M - H]^-$  ion at  $m/z$  595.16571, 595.16602 and 595.16382 (C<sub>27</sub>H<sub>33</sub>O<sub>15</sub>, error  $< 4$  ppm), respectively. These metabolites were 16 Da more massive than narirutin, which indicated that an oxidation reaction may have occurred. At the same time, DFICs at  $m/z$  287.06 ( $[M - C_{12}H_{20}O_9 + O]^-$ ,  $m/z$  271.06 + 15.99),  $m/z$  151.00,  $m/z$  135.04 ( $m/z$  119.05 + 15.99) were observed, which suggested that the oxidation site occurred in the B ring or at C-3. **M8**, **M10** and **M22** were identified as single increased oxygen oxidation products.

**M21** generated the  $[M - H]^-$  ion at  $m/z$  611.16010 (C<sub>27</sub>H<sub>31</sub>O<sub>15</sub>, error = -0.918 ppm) with a retention time of 5.90 min, and it was 32 Da more massive than narirutin, which

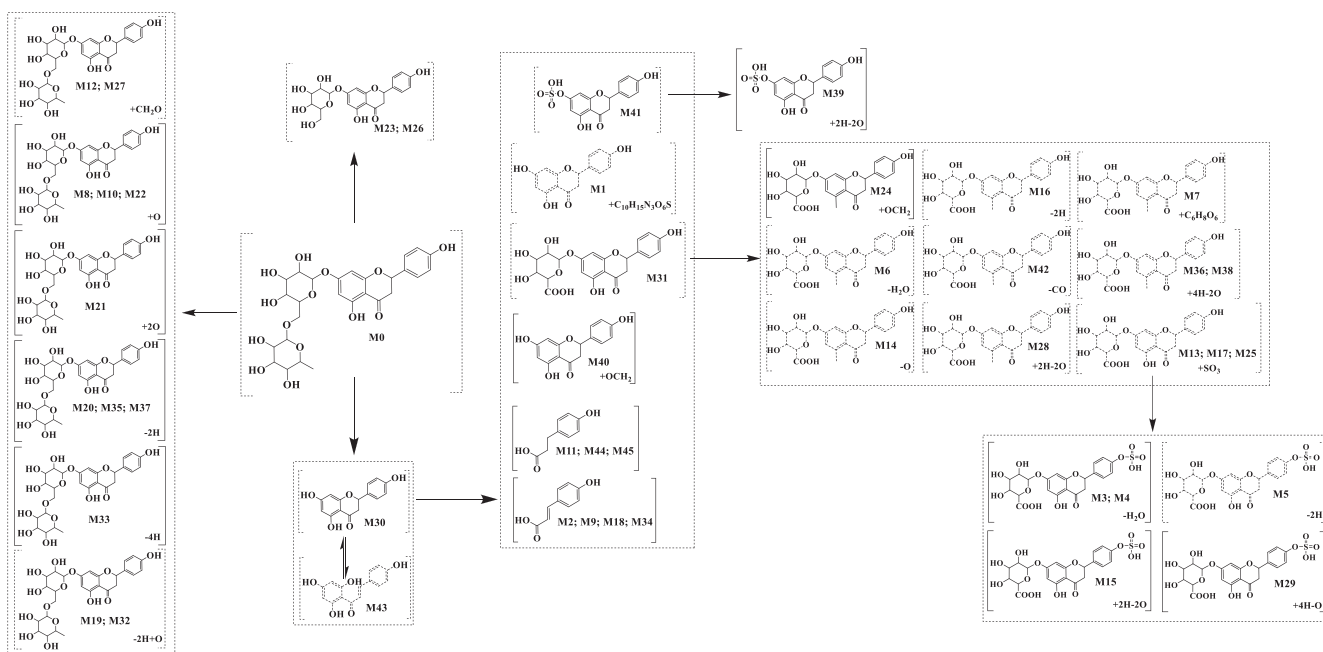


Fig. 5 Metabolic Pathway Profiling and Verification.

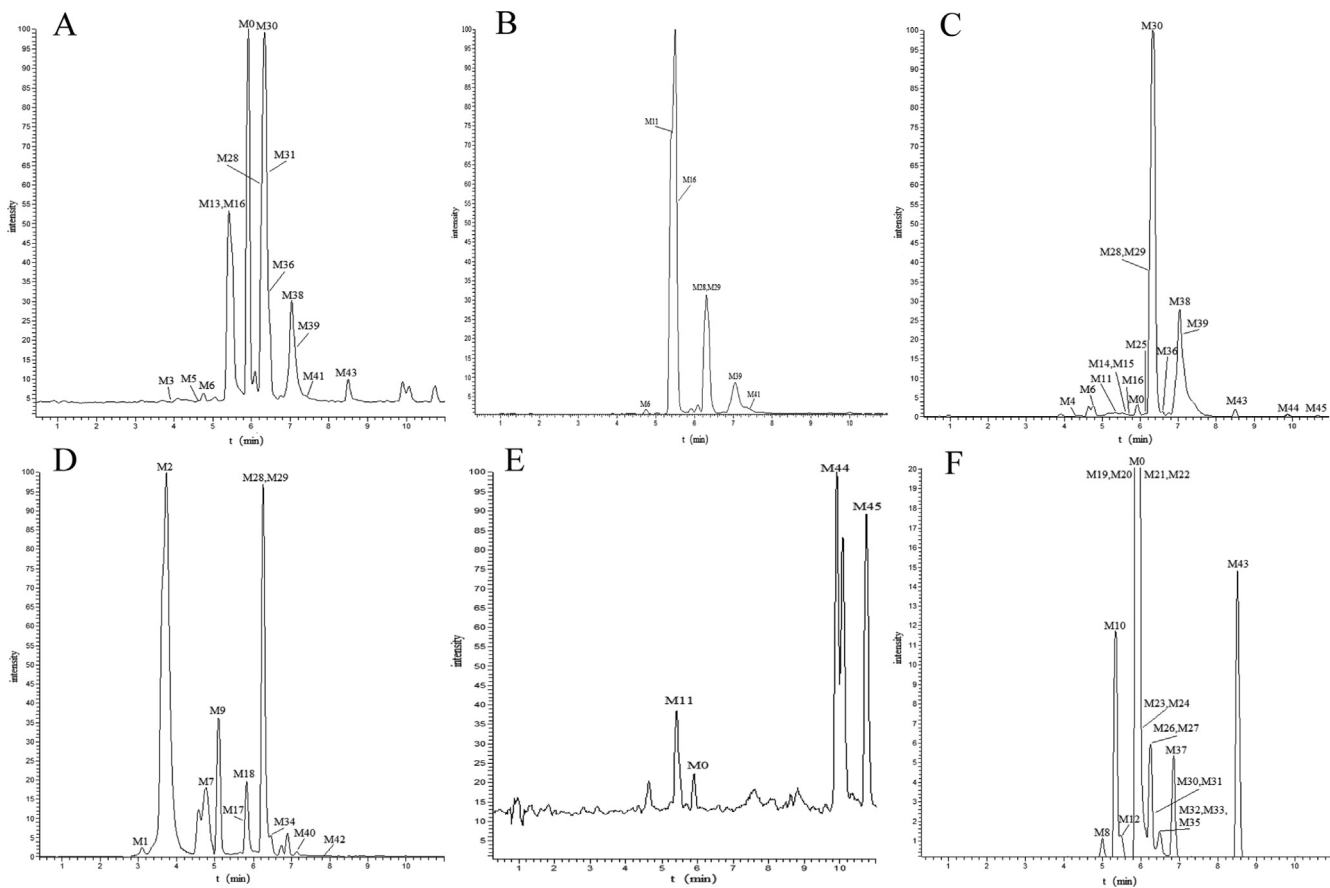


Fig. 6 The EIC profiles of the metabolites in the different samples (A: PS, plasma SPE extraction; B: PM, plasma methanol precipitation; C: PA, plasma acetonitrile precipitation; D: U, urine SPE extraction; E: LS, liver SPE extraction; F: LM, Prototype drug liver microsomal treatment).

suggested that **M21** was a double increased oxygen oxidation product of narirutin. According to the DFICs at  $m/z$  611.16 ( $m/z$  579.17 + 31.99),  $m/z$  303.05 ( $m/z$  271.06 + 31.99) and  $m/z$  151.00, the oxidation reaction occurred on aglycone and not on the A ring. Based on the unique cracking law (Yang et al., 2015) of flavonoid compounds, the CSIs at  $m/z$  285.04 ( $[M-H-C_6H_{12}O_4-H_2O]^+$ ) and  $m/z$  269.04 ( $[M-H-C_6H_{12}O_4-H_2O-O]^+$ ) were compared. Thus, **M21** was deduced as 3, 6'-OH-narirutin.

**M20** generated its  $[M-H]^-$  ion at  $m/z$  577.15515 with a mass error of  $-0.055$  ppm and its  $[M + H]^+$  ion at 579.17004 with a mass error of  $-1.367$  ppm. At the same time, DFICs at  $m/z$  151.00 (-),  $m/z$  93.03 (-) and  $m/z$  153.02 (+) were observed. The CSIs at  $m/z$  269.04 in the negative ion mode and  $m/z$  271.06 in the positive ion mode were 2 Da smaller than narirutin, which indicated that dehydrogenation occurred on aglycones. **M20** was tentatively inferred as 7-rutinoside-apigenin. However, due to the lack of sufficient fragment ion information, we were unable to confirm that its aglycone was apigenin, indicating that the specific structure of **M20** requires further experimental investigation. **M37** was 2 Da less massive than narirutin. However, the DFICs at  $m/z$  271.06,  $m/z$  151.00 and  $m/z$  119.05 in the negative ion mode as well as  $m/z$  273.07 and  $m/z$  153.02 in the positive ion mode were the same as those of narirutin, which indicated that the dehydrogenation reaction occurred at the rutinoside group. Thus, **M20** and **M37** were metabolites produced by the dehydrogenation of rutinoside groups.

**M19** and **M32** with the same theoretical  $[M + H]^+$  ions at  $m/z$  595.16575 ( $C_{27}H_{30}O_{15}$ , mass error within 4 ppm) were observed at 5.88 min and 6.46 min, respectively. In the ESI-MS/MS spectrum of **M19**, the CSIs at  $m/z$  287.05 ( $m/z$  273.07 + 13.98) could indicate that the oxidation has occurred in the aglycone group. The DFICs of **M32** such as those at  $m/z$  435.13 ( $[M + H-C_6H_{12}O_4]^+$ ),  $m/z$  273.07 ( $[M + H-C_{27}H_{30}O_{14}]^+$ ),  $m/z$  153.02 and 147.04 provided evidences to help us determined where the oxidation occurred in the rutinoside site. Thus, **M19** and **M32** were deduced as the dehydrogenation and oxygenation metabolites of narirutin.

**M12** and **M27** possessed identical  $[M-H]^-$  ions at  $m/z$  609.18249 ( $C_{28}H_{34}O_{15}$ , error < 4 ppm) with retention times of 5.45 min and 6.26 min, respectively. Presumably they were from the oxidation of narirutin. They were 30 Da more massive than Narirutin. Presumably, they were hydroxylation and methylation products of narirutin. In the ESI-MS/MS spectrum, **M12** showed its DFICs at  $m/z$  271.06 ( $[M-H-C_6H_{12}O_4]^-$ ),  $m/z$  119 and  $m/z$  93.03 and CSIs at  $m/z$  301.07 ( $[M-H-C_6H_{12}O_4 + OCH_2]^-$ ),  $m/z$  283.06 ( $[M-H-C_6H_{12}O_4 + OCH_2-H_2O]^-$ ). It was proved that the hydroxylation and methylation reaction took place in the A ring. The DFICs and CSIs at  $m/z$  301.07 ( $[M-H-C_6H_{12}O_4]^-$ ),  $m/z$  271.06 ( $[M-H-C_6H_{12}O_4-OCH_2]^-$ ),  $m/z$  151.00 and  $m/z$  149.06 ( $m/z$  119.05 + 30.01) could be determined that the hydroxylation and methylation reaction of **M27** occurred in the B ring. Thus, **M12** and **M27** were tentatively identified as the hydroxylation and methylation products of Narirutin.

### 3.3.2. Identification of naringenin and naringenin Chalcone's metabolites

**M1** was eluted at 3.15 min and showed its  $[M-H]^-$  ion at  $m/z$  576.13464 ( $C_{25}H_{27}O_{11}N_3S$ , error = 1.081). It was 305 Da more

than **M30** and **M43**, indicating that one of them were glutathione (GSH) binding product. In the ESI-MS/MS spectrum, the DFICs at  $m/z$  271.06,  $m/z$  151.00 and  $m/z$  119.05 from narirutin and at  $m/z$  447.09 ( $[M-H-C_5H_7O_3N]^-$ ),  $m/z$  400.10 ( $[M-H-C_5H_7O_3N-CH_4S]^-$ ),  $m/z$  74.02 ( $[C_2H_4NO_2]^-$ ),  $m/z$  59.01 ( $[C_2H_3O_2]^-$ ) from Glutathione group provided evidence that **M1** was glutathionated metabolites.

In the negative ion mode, metabolite **M31** possessed  $[M-H]^-$  ion at  $m/z$  447.09328 ( $C_{21}H_{20}O_{11}$ , error = 0.564) with the retention time of 6.35 min. It was 176 Da more than naringenin. The DFICs at  $m/z$  271.06 ( $[M-H-GluA]^-$ ),  $m/z$  175.02 ( $[GluA-H]^-$ ),  $m/z$  151.00,  $m/z$  119.05,  $m/z$  113.02 ( $[GluA-H-CH_2O_3]^-$ ) and  $m/z$  93.03, suggesting the present of glucuronidation. By comparing the ClogP value and retention time of metabolites **M30** and **M43**, it can be determined that **M31** is the glucoaldehyde acid product of naringenin chalcone (**M43**).

**M40** ( $C_{16}H_{14}O_6$ , error = 1.247) was 30 Da more massive than **M30** and **M43** and eluted at 7.14 min. The DFICs such as  $m/z$  301.07 ( $[M-H]^-$ ),  $m/z$  271.06 ( $[M-H-OCH_3]^-$ ) and  $m/z$  119.05 and the CSIs at  $m/z$  181.05 ( $m/z$  151.00 + 30.05) suggested that **M40** was identified as the methoxylation product of **M30** and **M43** and the  $OCH_2$  group may be introduced into the A ring. According to the retention time and ClogP value, **M40** was tentatively deduced as the methoxylation product of naringenin (**M30**).

**M41** generated the ion at  $m/z$  351.01727 ( $C_{15}H_{12}SO_8$ , error = 1.013) with the retention time of 7.40 min. It was 80 Da more massive than **M30** and **M43**, indicating that it might be the sulfated product of them. The DFICs such as  $m/z$  271.06 ( $[M-H-SO_3]^-$ ),  $m/z$  151.00, 119.05,  $m/z$  93.03 and  $m/z$  79.96 ( $[SO_3]^-$ ) could prove that **M41** was the sulfated product of **M30** and **M43**. The introduction of sulfate group will increase the polarity of the prototype compound. The final identification will be based on the comparison between the polarity and ClogP value of the compound. Therefore, **M41** was identified as the sulfated product of naringenin chalcone (**M43**).

### 3.3.3. Identification of naringenin glucuronidation metabolites

**M7** was eluted at 4.79 min and was 176 Da more massive than **M31**. The deprotonation ion at  $m/z$  623.12537 ( $C_{27}H_{28}O_{17}$ , error = 0.569) was generated. In addition, the DFICs involving  $m/z$  447.09 ( $[M-H-GluA]^-$ ),  $m/z$  271.06 ( $[M-H-2GluA]^-$ ),  $m/z$  175.02 ( $[GluA-H]^-$ ),  $m/z$  151.00,  $m/z$  119.05,  $m/z$  113.02 ( $[GluA-H-CH_2O_3]^-$ ) and  $m/z$  93.03 were identical to those of **M31**. Thus, **M7** was identified as the glucuronidation product of **M31** [double glucuronidation product of naringenin chalcone (**M43**)].

**M13**, **M17** and **M25** were 80 Da more than **M31**. They were presumed to be sulfated products of **M31**. They showed the theoretical  $[M-H]^-$  ion at 527.05010 ( $C_{21}H_{20}O_{14}S$ , error < 4). The DFICs at  $m/z$  271.06 ( $[M-H-SO_3-GluA]^-$ ),  $m/z$  175.02,  $m/z$  151.00,  $m/z$  119.05,  $m/z$  113.02 and the CSIs at  $m/z$  447.09 ( $[M-H-SO_3]^-$ ),  $m/z$  351.02 ( $[M-H-GluA]^-$ ) indicated that glucuronic acid and sulfate were combined at different locations of **M31**, respectively. It could be inferred that **M13**, **M17** and **M25** were products of glucuronidation and sulfate of **M31**.

Reduction reactions also occur in living organisms. **M28** generated the  $[M-H]^-$  ion at  $m/z$  417.11911 ( $C_{21}H_{22}O_9$ , error = 1.466) with the retention time of 6.26 min. The DFICs

such as  $m/z$  175.02,  $m/z$  113.02,  $m/z$  119.05 and  $m/z$  93.03, could infer that the reduction reaction did not happen in the glucuronic group and the B ring. But, according to the CSIs at  $m/z$  241.09,  $m/z$  135.04 and  $m/z$  121.03, we could finally deduce that **M28** was the hydrogenation and double-deoxidized product of **M31** and the reduction reaction occurred in the A ring. **M36** and **M38** with theoretical  $[M-H]^-$  ions at 419.134 ( $C_{21}H_{24}O_9$ , mass error within 4 ppm) were observed at 6.57 min and 7.03 min, respectively. Their reaction site and the DFICs were similar to that of **M28** and one step more hydrogenation reduction reaction occurred than that of **M28**. Finally, they were identified as the double deoxygenation and hydrogenation metabolites of **M31**. In a similar way, **M14** eluted at 5.59 min and gave rise to a  $[M-H]^-$  ion at  $m/z$  431.09219 ( $C_{21}H_{20}O_{10}$ , error = 0.828). It was 16 Da less massive than **M31**. In the ESI-MS/MS spectrum, the DFICs such as these at  $m/z$  255.06 ( $[M-H-GluA-O]^-$ ),  $m/z$  175.02 ( $[GluA-H]^-$ ) and  $m/z$  113.02 ( $[GluA-H-CH_2O_3]^-$ ), supported our to identify it as the deoxygenation product of **M31**.

**M16** with the  $[M + H]^+$  ion at  $m/z$  447.09219 ( $C_{21}H_{18}O_{11}$ , the mass error -1.225 ppm) was observed at 5.70 min. It was 2 Da less massive than **M31**. The DFICs and CSIs at  $m/z$  271.06 and  $m/z$  153.02, could support us to deduce that **M16** was the dehydrogenation product of **M31**.

**M6** was 18 Da less massive than **M31**. It eluted at 4.73 min and its formula was speculated as  $C_{21}H_{18}O_{10}$ , with the mass error of 0.878. According to the DFICs at  $m/z$  429.08 ( $[M-H]^-$ ),  $m/z$  253.05 ( $m/z$  271.06-18.01),  $m/z$  175.02 and  $m/z$  113.02, indicating that **M6** was the dehydration product of **M31**.

**M42** with the ion at  $m/z$  421.11292 ( $C_{20}H_{20}O_{10}$ , error = -1.274) was observed at 7.83 min. It was 28 less massive than **M31** and presumed to be a metabolite formed by **M31** took off the carbonyl group. The DFICs at  $m/z$  245.05 and  $m/z$  121.03 further indicated that **M42** was the decarbonyl product of **M31**.

**M24** was eluted at 6.05 min and was 30 Da more massive than **M31**. It showed its  $[M + H]^+$  ion at  $m/z$  479.11840 ( $C_{22}H_{22}O_{12}$ , error = -1.508). In its ESI-MS/MS spectrum, the DFICs and CSIs at  $m/z$  303.09 ( $[M + H + OCH_2]^+$ ), 183.03 ( $m/z$  153.02 + 30.01),  $m/z$  147.04 and  $m/z$  136.06, could indicate that  $OCH_2$  groups were introduced into the A ring. **M24** was finally identified as the methoxylation product of **M31**.

### 3.3.4. Identification of naringenin sulfate metabolites

**M39** generated the ion at  $m/z$  321.04330 ( $C_{15}H_{14}SO_6$ , error = 1.759) with the retention time of 7.06 min. It was 30 Da less massive than **M41**. Because the **M39** did not have a  $-OCH_3$  group. The DFICs such as  $m/z$  241.09 ( $m/z$  271.06-29.97),  $m/z$  121.03 ( $m/z$  151.00-29.97),  $m/z$  119.05 and  $m/z$  93.03 were deduced that **M39** was the hydrogenation and double-deoxidized metabolite of **M41** and the reaction happened in the A ring.

### 3.3.5. Identification of naringenin glucuronidation and sulfate metabolites

**M3** and **M4** possessed the same theoretical ion at  $m/z$  509.03953 ( $C_{21}H_{18}SO_{13}$ , error < 4) in the negative ion mode. These metabolites were 18 Da less massive than **M13**, **M17**

and **M25**, indicating that they might be the dehydration product. The dehydration reaction occurred on the basis of glucuronidation and sulfate according to the DFICs at  $m/z$  333.01 ( $[M-H-GluA]^-$ ),  $m/z$  253.05 ( $[M-H-GluA-SO_3]^-$ ),  $m/z$  113.02 ( $[GluA-H-CH_2O_3]^-$ ) and  $m/z$  79.96 ( $[SO_3]^-$ ). Binding the CSIs at  $m/z$  253.05 ( $m/z$  271.06-18.01), **M3** and **M4** were tentatively identified as the dehydration product of **M13**, **M17** and **M25**.

**M5** eluted at 4.64 min and was 2 Da less than **M13**, **M17** and **M25**. Combined with the DFICs at  $m/z$  445.08 ( $[M-H-SO_3]^-$ ),  $m/z$  349.00 ( $[M-H-GluA]^-$ ) and  $m/z$  269.04 ( $[M-H-GluA-SO_3]^-$ ), **M5** was finally deduced as the dehydrogenation product of **M13**, **M17** and **M25**.

**M15** generated the ion at  $m/z$  497.07592 ( $C_{21}H_{22}O_{12}S$ , error = 1.759) with the retention time of 5.63 min. It was 30 Da less massive than **M13**, **M17** and **M25**. The DFICs such as these  $m/z$  321.04 ( $[M-H-GluA]^-$ ),  $m/z$  241.09 ( $[M-H-GluA-SO_3]^-$ ),  $m/z$  175.02,  $m/z$  119.05,  $m/z$  113.02 and  $m/z$  79.96 provided evidence to infer that **M15** was the metabolites of **M13**, **M17** and **M25**. And according to the CSIs at  $m/z$  241.09 ( $m/z$  271.06-29.97),  $m/z$  135.04 and  $m/z$  121.03 ( $m/z$  151.00-29.97), it was proved that the reduction reaction occurred in the A ring. Finally, **M15** was identified as the hydrogenation and double-deoxidized metabolite of **M13**, **M17** and **M25**.

**M29** eluted at 6.27 min and showed its  $[M-H]^-$  ion at  $m/z$  515.08 ( $C_{21}H_{24}SO_{13}$ , error = -3.083). Observations of its DFICs at  $m/z$  271.06,  $m/z$  151.00,  $m/z$  119.05 and  $m/z$  79.96 were found that reduction reaction did not occur on aglycone and Sulfate group. Therefore, it was preliminarily speculated that the reduction reaction took place at the glucuronidation group. Thus, **M29** was characterized as the deoxygenation and double-hydrogenation product of **M13**, **M17** and **M25**.

### 3.3.6. Identification of naringenin other metabolites

According to the data, naringin can generate aglycon naringin under the action of intestinal flora. And naringenin can generate p-hydroxyphenylpropionic acid, p-hydroxycinnamic acid and their isomers through ring-opening reaction under the microorganism (Liu et al., 2012; Zeng et al., 2020a, 2020b). It is speculated that narirutin can also have similar reaction. **M11**, **M44** and **M45** were possessed the same theoretical  $[M-H]^-$  ions at  $m/z$  165.05572 ( $C_9H_{10}O_3$ , error < 4 ppm) in the negative ion mode, respectively. The fragment ions such as  $m/z$  147.04 ( $[M-H-H_2O]^-$ ),  $m/z$  121.06 ( $[M-H-CO_2]^-$ ) and 119.05 were exhibited in the ESI-MS/MS spectra. Hence, **M11**, **M44** and **M45** were identified as p-Hydroxyphenylpropionic acid and their isomers. **M2**, **M9**, **M18** and **M34** were 2 Da less massive than **M11**, **M44** and **M45**. Therefore, it was speculated that they were metabolites formed by dehydrogenation of **M11**, **M44** and **M45** in the liver. Identify them according to the fragment ions at  $m/z$  163.04007 ( $[M-H]^-$ ),  $m/z$  119.05 and  $m/z$  93.03, **M2**, **M9**, **M18** and **M34** were eventually identified as p-hydroxycinnamic acid and their isomers.

## 4. Discussion

In previous literatures, we found that many researches primarily focus on pharmacokinetics of narirutin. Bioavailability and route of excretion were studied in healthy humans after taking fruit juice (Brett et al., 2009; Silveira et al., 2014; Aschoff et al.,

2016) or rats oral drugs containing narirutin (Zhang et al., 2018; Li et al., 2019; Fu et al., 2020). Zhang et al. studied after human consumption of grapefruit juice (the main flavonoids were naringin and narirutin), screened flavonoid metabolites from urine, and found that 9 metabolites were naringenin glucuronides, naringenin sulfates, naringenin glucuronide sulfates and naringenin diglucuronide and their isomers (Zhang and Brodbelt 2004). The above studies indicated that it was not enough for studying the metabolites of narirutin.

In the present study, the *in vitro* and *in vivo* metabolism of narirutin was studied in SD rats, including in rat plasma (three different treatments (Jordan et al., 2009)), urine (Nema et al., 2010), faeces, liver tissues and liver microsomes (Knights et al., 2016), to obtain as many narirutin metabolites as possible. The relevant information of each metabolite was captured in positive and negative ion modes by UPLC-Q-Exactive Orbitrap MS/MS after oral administration of narirutin. Combined with the chromatographic retention behavior, accurate molecular weight, positive and negative ion cleavage modes and the cleavage rules of the reference product, a total of 46 metabolites (including prototype drugs) were identified. A total of 22 metabolites were identified in rat plasma, including 16, 13 and 8 metabolites identified from solid phase extraction (SPE), acetonitrile treatment and methanol treatment, respectively. In addition, the metabolites treated with methanol were found in the products of the other two sample treatments, which indicated that the results of plasma samples treated with methanol were not ideal. Therefore, the combination of SPE and acetonitrile treatment may provide a more comprehensive characterization of plasma metabolites.

Based on the above results, we found that the metabolic pathways of narirutin *in vitro* and *in vivo* were different. Only three metabolites (M30, M31 and M43) *in vivo* had similar metabolic pathways *in vitro*. Narirutin was decomposed to its aglycones, namely, naringenin and naringenin chalcone, *in vivo* (M30 and M43, the relative content was abundant). Naringenin and naringenin chalcone produced a series of metabolites, such as glucuronidation (M31), sulfation (M41) and glutathione binding (M1). On the basis of these metabolites, further oxidation, reduction, dehydration, decarbonylation and other reactions occurred. Another pathway occurred, in which naringenin and naringenin chalcone were cleaved by the microbiota-mediated ring fission of unabsorbed flavonoids to produce p-hydroxyphenylpropionic acid, p-hydroxycinnamic acid and their isomers, as well as the metabolites excreted by enterohepatic circulation (Zeng et al., 2020a, 2020b). This was precisely why we found them only in metabolites *in vivo*, but not in the metabolism of liver microsomes, because of the lack of the ring-opening effect from intestine microorganism. Therefore, we found p-hydroxyphenylpropionic acid and its isomers (M11, M44 and M45) in plasma and liver tissues, and we found p-hydroxycinnamic acid and its isomers (M2, M9, M18 and M34) in urine. Therefore, these findings suggested that p-hydroxyphenylpropionic acid and its isomers were further transformed to p-hydroxycinnamic acid and its isomers, which were excreted from the body. In addition, the relative contents of these compounds in the body were high, suggesting that this metabolic pathway is one of the main metabolic pathways of narirutin *in vivo*. Regarding the *in vitro* metabolites, most of the metabolites in liver microsomes were based on the metabolic reactions of narirutin, including oxidation, reduction,

hydroxylation and methylation reactions. In liver microsomes, we found that the M23 and M26 metabolites were compounds on naringenin that could bind only one glucose. Therefore, we speculated that there may be two generation paths as follows: one was formed by the removal of rhamnose from narirutin, and the other was that narirutin was broken down into naringenin, which was then combined with glucose. In the *in vitro* and *in vivo* metabolic pathways, a prototype drug was found. The relative content of narirutin was the highest in plasma followed by urine, and the relative content of narirutin in liver microsomes was also relatively abundant. Therefore, the prototype drug was metabolized and eliminated from the body, which was also one of the main metabolic forms of narirutin. Finally, we concluded that the main difference between *in vitro* and *in vivo* metabolism of narirutin lies in the time and degree of its metabolism. *In vivo* experiments, after three days of intragastric administration, a large number of drugs entered the body of rats, and metabolic reactions fully occurred. Therefore, we not only found primary metabolites of narirutin, but also secondary and tertiary metabolites were also observed. Meanwhile, under the action of intestinal flora, the ring-opening reaction of narirutin and its metabolites were promoted, which enriched the metabolic spectrum of narirutin *in vivo*. However, *in vitro*, the liver microsomes experiment was administered only once and conducted for 240 min, which did not allow sufficient time for deeper reactions. Therefore, most of the reactions were based on the primary metabolites of narirutin, and few secondary metabolites were produced.

In the present study, an analysis strategy based on ACR, DFICs and CSIs was proposed to rapidly identify narirutin metabolites. This strategy can be applied not only to the identification of narirutin metabolites in the present study but also to the identification of other flavonoid metabolites, even saponins and alkaloids. For these compounds with a basic core structure, this strategy can be used to quickly identify metabolites from LC-MS information. The fragmentation law of the core structure of the compound is summarized to obtain the corresponding fragment ions. According to the functional groups bound to the compound, the fragmentation ion clusters of the compound are deduced, which are called DFICs. The accuracy of DFICs are tested by the cracking information of the reference substance. Accurate DFICs information facilitates the rapid identification of metabolites. According to the structural information and metabolic characteristics of compounds *in vivo*, the possible main metabolites are deduced. Based on this node, the possible metabolites are deduced by the recurrence formula. The metabolites are identified by combining the DFICs and secondary fragment information. Further, suggestive fragment ions, called CSIs, are identified from the DFICs to preliminarily infer the sites where metabolic reactions occur, and the metabolites are then identified.

Several major metabolites produced during metabolism may be part of the related pharmacological effects of narirutin. Narirutin and the metabolized forms of naringenin, including naringenin chalcone and naringenin chalcone glucuronidation, were detected *in vivo* and *in vitro*. The relative content of these compounds in the metabolites *in vivo* were abundant, indicating that they are the key metabolites in the metabolic process of narirutin. Recent studies have reported that naringenin has a variety of pharmacological effects similar to narirutin, such as anti-inflammatory, antiviral (Tutunchi et al., 2020) and antidiabetic (Den Hartogh and Tsiani 2019) effects. Thus, nar-

irutin possesses pharmacological effects, in part, due to its metabolism in the body to produce naringenin. Naringenin also has potential immunomodulatory effects (Zeng et al., 2018) and regulatory effects in nonalcoholic fatty liver disease (Wang et al., 2020; Hua et al., 2021). Escribano-ferrer et al. reported that naringenin chalcone may be a useful alternative for topical treatment of inflammatory and allergic skin diseases. The present study linked the metabolism and pharmacological effects of narirutin *in vivo*, suggesting that studies on narirutin are warranted (Escribano-Ferrer et al., 2019). Citrus peel extract has a positive effect on fat production and breakdown (Chou et al., 2018), and one of the main components of citrus peel extract is narirutin. Horiba et al. reported that narirutin improves adipocyte metabolic functions and exerts insulin-sensitizing effects by activating an adiponectin-related pathway. Therefore, these findings suggest that naringenin chalcone may be the key metabolite of narirutin in improving adipocyte function (Horiba et al., 2010). Kolot et al. reported that naringenin chalcone is bioavailable in humans from a dietary source but that its availability is poor. The intramolecular cyclisation and extended metabolism of naringenin chalcone likely contribute to the inactivation of the  $\alpha,\beta$ -unsaturated reactive center and the excretion of the biologically active molecule, respectively, which may explain the paucity of studies on naringenin chalcone (Kolot et al., 2020).

## 5. Conclusion

The present study comprehensively characterized the metabolites of narirutin *in vitro* and *in vivo*, which provided a basis to study the pharmacological activity mechanism of narirutin. In addition, the present study proposed a new analysis strategy for the rapid identification of metabolites, providing support for the study of compound metabolism.

The annotations of some abbreviations:

ACR: analogous core recursion, DFICs: diagnostic fragment ion clusters, CSIs: characteristic suggestive ions, EIC: Extracted Ion Chromatography, SPE: Solid Phase Extraction, UHPLC: ultra-high-performance Liquid Chromatography, MS: Mass Spectrum, GluA: glucuronyl, Glc: glucosyl.

## CRedit authorship contribution statement

**Shuyi Song:** Methodology, Writing – original draft. **Hongyan Zhou:** Methodology. **Xianming Lan:** Methodology. **Xiaoqing Yuan:** Methodology. **Yanan Li:** . **Shuteng Huang:** . **Zhibin Wang:** Conceptualization, Funding acquisition, Project administration, Methodology, Supervision. **Jiayu Zhang:** Conceptualization, Funding acquisition, Project administration, Methodology, Supervision.

## Declaration of Competing Interest

The authors declare that they have no known competing financial interests or personal relationships that could have appeared to influence the work reported in this paper.

## Acknowledgments

This work has been financially supported by Shandong Taishan Scholars Young Expert Project (tsqn202103110), Shan-

dong Province Youth Talents Introducing and Cultivating Program-Innovative Research Team (10073004), Supporting plan for leading talents above provincial level in Yantai (10073801).

## References

- Aschoff, J.K., Riedl, K.M., Cooperstone, J.L., et al, 2016. Urinary excretion of Citrus flavanones and their major catabolites after consumption of fresh oranges and pasteurized orange juice: A randomized cross-over study. *Mol. Nutr. Food Res.* 60, 2602–2610. <https://doi.org/10.1002/mnfr.201600315>.
- Brett, G.M., Hollands, W., Needs, P.W., et al, 2009. Absorption, metabolism and excretion of flavanones from single portions of orange fruit and juice and effects of anthropometric variables and contraceptive pill use on flavanone excretion. *Br. J. Nutr.* 101, 664–675. <https://doi.org/10.1017/s000711450803081x>.
- Chiechio, S., Zammataro, M., Barresi, M., et al, 2021. A Standardized Extract Prepared from Red Orange and Lemon Wastes Blocks High-Fat Diet-Induced Hyperglycemia and Hyperlipidemia in Mice. *Molecules* (Basel, Switzerland). 26. <https://doi.org/10.3390/molecules26144291>.
- Chou, Y.C., Ho, C.T., Pan, M.H., 2018. Immature Citrus reticulata Extract Promotes Browning of Beige Adipocytes in High-Fat Diet-Induced C57BL/6 Mice. *J. Agric. Food Chem.* 66, 9697–9703. <https://doi.org/10.1021/acs.jafc.8b02719>.
- Den Hartogh, D.J., Tsiani, E., 2019. Antidiabetic Properties of Naringenin: A Citrus Fruit Polyphenol. *Biomolecules* 9. <https://doi.org/10.3390/biom9030099>.
- Duan, L., Guo, L., Dou, L.L., et al, 2016. Discrimination of Citrus reticulata Blanco and Citrus reticulata 'Chachi' by gas chromatograph-mass spectrometry based metabolomics approach. *Food Chem.* 212, 123–127. <https://doi.org/10.1016/j.foodchem.2016.05.141>.
- Escribano-Ferrer, E., Queralt Regué, J., Garcia-Sala, X., et al, 2019. In Vivo Anti-inflammatory and Antiallergic Activity of Pure Naringenin, Naringenin Chalcone, and Quercetin in Mice. *J. Nat. Prod.* 82, 177–182. <https://doi.org/10.1021/acs.jnatprod.8b00366>.
- Fraga, L.N., Coutinho, C.P., Rozenbaum, A.C., et al, 2021. Blood pressure and body fat % reduction is mainly related to flavanone phase II conjugates and minor extension by phenolic acid after long-term intake of orange juice. *Food Funct.* 12, 11278–11289. <https://doi.org/10.1039/d1fo02664j>.
- Fu, C., Wu, Q., Zhang, Z., et al, 2020. Development of a sensitive and rapid UHPLC-MS/MS method for simultaneous quantification of nine compounds in rat plasma and application in a comparative pharmacokinetic study after oral administration of Xuefu Zhuyu Decoction and nimodipine. *Biomedical chromatography : BMC.* 34, e4872.
- Ha, S.K., Park, H.Y., Eom, H., et al, 2012. Narirutin fraction from citrus peels attenuates LPS-stimulated inflammatory response through inhibition of NF- $\kappa$ B and MAPKs activation. *Food Chem. Toxicol.* 50, 3498–3504. <https://doi.org/10.1016/j.fct.2012.07.007>.
- Horiba, T., Nishimura, I., Nakai, Y., et al, 2010. Naringenin chalcone improves adipocyte functions by enhancing adiponectin production. *Mol. Cell. Endocrinol.* 323, 208–214. <https://doi.org/10.1016/j.mce.2010.03.020>.
- Hua, Y.Q., Zeng, Y., Xu, J., et al, 2021. Naringenin alleviates nonalcoholic steatohepatitis in middle-aged Apoe(-/-)mice: role of SIRT1. *Phytomedicine : international journal of phytotherapy and phytopharmacology.* 81., <https://doi.org/10.1016/j.phymed.2020.153412> 153412.
- Jiang, S., Wang, S., Dong, P., et al, 2021. A comprehensive profiling and identification of liquiritin metabolites in rats using ultra-high-performance liquid chromatography coupled with linear ion trap-orbitrap mass spectrometer. *Xenobiotica; the fate of foreign*

- compounds in biological systems. 51, 564–581. <https://doi.org/10.1080/00498254.2020.1854366>.
- Jordan, T.B., Nichols, D.S., Kerr, N.I., 2009. Selection of SPE cartridge for automated solid-phase extraction of pesticides from water followed by liquid chromatography-tandem mass spectrometry. *Anal. Bioanal. Chem.* 394, 2257–2266. <https://doi.org/10.1007/s00216-009-2924-4>.
- Knights, K.M., Stresser, D.M., Miners, J.O., et al, 2016. In Vitro Drug Metabolism Using Liver Microsomes. *Curr. Protocols Pharmacol.* 74, 7.8.1–7.8.24. <https://doi.org/10.1002/cpph.9>.
- Kolot, C., Rodriguez-Mateos, A., Feliciano, R., et al, 2020. Bioavailability of naringenin chalcone in humans after ingestion of cherry tomatoes. *International journal for vitamin and nutrition research. Internationale Zeitschrift für Vitamin- und Ernährungsforschung. Journal international de vitaminologie et de nutrition.* 90, 411–416. <https://doi.org/10.1024/0300-9831/a000574>.
- Lan, X., Li, Y., Li, H., et al, 2022. Drug metabolite cluster centers-based strategy for comprehensive profiling of Neomangiferin metabolites *in vivo* and *in vitro* and network pharmacology study on anti-inflammatory mechanism. *Arab. J. Chem.* 15. <https://doi.org/10.1016/j.arabjc.2022.104268>.
- Li, P., Zeng, S.L., Wang, Z.Y., et al, 2019. Simultaneous Quantification of Five Flavanone Glycosides in Rat Plasma by Ultra-Performance Liquid Chromatography-Tandem Mass Spectrometry: Application to a Comparative Pharmacokinetic Study of Aurantii Fructus Immaturus and Aurantii Fructus Extracts. *J. AOAC Int.* 102, 781–787. <https://doi.org/10.5740/jaoacint.18-0285>.
- Lim, H., Yeo, E., Song, E., et al, 2015. Bioconversion of Citrus unshiu peel extracts with cytolase suppresses adipogenic activity in 3T3-L1 cells. *Nutr. Res. Pract.* 9, 599–605. <https://doi.org/10.4162/nrp.2015.9.6.599>.
- Liu, M., Zou, W., Yang, C., et al, 2012. Metabolism and excretion studies of oral administered naringin, a putative antitussive, in rats and dogs. *Biopharm. Drug Dispos.* 33, 123–134. <https://doi.org/10.1002/bdd.1775>.
- Miles, E.A., Calder, P.C., 2021. Effects of Citrus Fruit Juices and Their Bioactive Components on Inflammation and Immunity: A Narrative Review. *Front. Immunol.* 12. <https://doi.org/10.3389/fimmu.2021.712608>.
- Mohanty, S., Konkimalla, V.B., Pal, A., et al, 2021. Naringin as Sustained Delivery Nanoparticles Ameliorates the Anti-inflammatory Activity in a Freund's Complete Adjuvant-Induced Arthritis Model. *ACS Omega* 6, 28630–28641. <https://doi.org/10.1021/acsomega.1c03066>.
- Nema, T., Chan, E.C., Ho, P.C., 2010. Application of silica-based monolith as solid phase extraction cartridge for extracting polar compounds from urine. *Talanta* 82, 488–494. <https://doi.org/10.1016/j.talanta.2010.04.063>.
- Niu, L., Wei, J., Li, X., et al, 2021. Inhibitory activity of narirutin on RBL-2H3 cells degranulation. *Immunopharmacol. Immunotoxicol.* 43, 68–76. <https://doi.org/10.1080/08923973.2020.1850764>.
- Park, H.Y., Ha, S.K., Eom, H., et al, 2013. Narirutin fraction from citrus peels attenuates alcoholic liver disease in mice. *Food Chem. Toxicol.* 55, 637–644. <https://doi.org/10.1016/j.fct.2013.01.060>.
- Qurtam, A.A., Mechchate, H., Es-Safi, I., et al, 2021. Citrus Flavanone Narirutin, *In Vitro* and *In Silico* Mechanistic Antidiabetic Potential. *Pharmaceutics.* 13. <https://doi.org/10.3390/pharmaceutics13111818>.
- Sahu, P.K., Mohapatra, P.K., Rajani, D.P., et al, 2020. Structure-based Discovery of Narirutin as a Shikimate kinase Inhibitor with Anti-tubercular Potency. *Curr. Comput. Aided Drug Des.* 16, 523–529. <https://doi.org/10.2174/1573409915666191025112150>.
- Shang, Z., Xin, Q., Zhao, W., et al, 2017. Rapid profiling and identification of puerarin metabolites in rat urine and plasma after oral administration by UHPLC-LTQ-Orbitrap mass spectrometer. *Journal of chromatography. B, Analytical technologies in the biomedical and life sciences.* 1068–1069, 180–192. <https://doi.org/10.1016/j.jchromb.2017.10.038>.
- Shehata, M.G., Awad, T.S., Asker, D., et al, 2021. Antioxidant and antimicrobial activities and UPLC-ESI-MS/MS polyphenolic profile of sweet orange peel extracts. *Current research in food science.* 4, 326–335. <https://doi.org/10.1016/j.crfs.2021.05.001>.
- Silveira, J.Q., Cesar, T.B., Manthey, J.A., et al, 2014. Pharmacokinetics of flavanone glycosides after ingestion of single doses of fresh-squeezed orange juice versus commercially processed orange juice in healthy humans. *J. Agric. Food Chem.* 62, 12576–12584. <https://doi.org/10.1021/jf5038163>.
- Tutunchi, H., Naeini, F., Ostadrahimi, A., et al, 2020. Naringenin, a flavanone with antiviral and anti-inflammatory effects: A promising treatment strategy against COVID-19. *Phytotherapy research : PTR.* 34, 3137–3147. <https://doi.org/10.1002/ptr.6781>.
- Wang, Q., Ou, Y., Hu, G., et al, 2020. Naringenin attenuates non-alcoholic fatty liver disease by down-regulating the NLRP3/NF- $\kappa$ B pathway in mice. *Br. J. Pharmacol.* 177, 1806–1821. <https://doi.org/10.1111/bph.14938>.
- Wong, E.S., Li, R.W., Li, J., et al, 2021. Relaxation effect of narirutin on rat mesenteric arteries via nitric oxide release and activation of voltage-gated potassium channels. *Eur. J. Pharmacol.* 905. <https://doi.org/10.1016/j.ejphar.2021.174190>.
- Wu, Y., Jiang, H., Chen, G., et al, 2021a. Preventive Effect of Gonggan (Citrus Reticulata Blanco Var. Gonggan) Peel Extract on Ethanol/HCl-Induced Gastric Injury in Mice via an Anti-oxidative Mechanism. *Front. Pharmacol.* 12. <https://doi.org/10.3389/fphar.2021.715306>.
- Wu, Y., Pan, L., Chen, Z., et al, 2021b. Metabolite Identification in the Preclinical and Clinical Phase of Drug Development. *Curr. Drug Metab.* 22, 838–857. <https://doi.org/10.2174/1389200222666211006104502>.
- Yang, R., Liu, H., Bai, C., et al, 2020. Chemical composition and pharmacological mechanism of Qingfei Paidu Decoction and Ma Xing Shi Gan Decoction against Coronavirus Disease 2019 (COVID-19): *In silico* and experimental study. *Pharmacol. Res.* 157. <https://doi.org/10.1016/j.phrs.2020.104820>.
- Yang, W.Z., Wu, W.Y., Yang, M., et al, 2015. Elucidation of the fragmentation pathways of a complex 3,7-O-glycosyl flavonol by CID, HCD, and PQD on an LTQ-Orbitrap Velos Pro hybrid mass spectrometer. *Chin. J. Nat. Med.* 13, 867–872. [https://doi.org/10.1016/s1875-5364\(15\)30091-1](https://doi.org/10.1016/s1875-5364(15)30091-1).
- Zeng, W., Jin, L., Zhang, F., et al, 2018. Naringenin as a potential immunomodulator in therapeutics. *Pharmacol. Res.* 135, 122–126. <https://doi.org/10.1016/j.phrs.2018.08.002>.
- Zeng, X., Yao, H., Zheng, Y., et al, 2020a. Metabolite Profiling of Naringin in Rat Urine and Feces Using Stable Isotope-Labeling-Based Liquid Chromatography-Mass Spectrometry. *J. Agric. Food Chem.* 68, 409–417. <https://doi.org/10.1021/acs.jafc.9b06494>.
- Zeng, X., Yao, H., Zheng, Y., et al, 2020b. Tissue distribution of naringin and derived metabolites in rats after a single oral administration. *J. Chromatogr. B, Anal. Technol. Biomed. Life Sci.* 1136. <https://doi.org/10.1016/j.jchromb.2019.121846>.
- Zhang, J., Brodbelt, J.S., 2004. Screening flavonoid metabolites of naringin and narirutin in urine after human consumption of grapefruit juice by LC-MS and LC-MS/MS. *Analyst* 129, 1227–1233. <https://doi.org/10.1039/b412577k>.
- Zhang, X., Han, L., Liu, J., et al, 2018. Pharmacokinetic Study of 7 Compounds Following Oral Administration of Fructus Aurantii to Depressive Rats. *Front. Pharmacol.* 9, 131. <https://doi.org/10.3389/fphar.2018.00131>.